



Industrial Robot: An International Journal

Development of a dexterous continuum manipulator for exploration and inspection in confined spaces
Shuntao Liu Zhixiong Yang Zhijun Zhu Liangliang Han Xiangyang Zhu Kai Xu

Article information:

To cite this document:

Shuntao Liu Zhixiong Yang Zhijun Zhu Liangliang Han Xiangyang Zhu Kai Xu , (2016), "Development of a dexterous continuum manipulator for exploration and inspection in confined spaces", Industrial Robot: An International Journal, Vol. 43 Iss 3 pp. 284 - 295

Permanent link to this document:

<http://dx.doi.org/10.1108/IR-07-2015-0142>

Downloaded on: 31 May 2016, At: 21:19 (PT)

References: this document contains references to 32 other documents.

To copy this document: permissions@emeraldinsight.com

The fulltext of this document has been downloaded 57 times since 2016*

Users who downloaded this article also downloaded:

(2016), "Hybrid position/force control of 6-dof hydraulic parallel manipulator using force and vision", Industrial Robot: An International Journal, Vol. 43 Iss 3 pp. 274-283 <http://dx.doi.org/10.1108/IR-10-2015-0192>

(2016), "Kinematic calibration of parallel manipulator with full-circle rotation", Industrial Robot: An International Journal, Vol. 43 Iss 3 pp. 296-307 <http://dx.doi.org/10.1108/IR-08-2015-0161>

(2016), "Flexible and soft robotic grippers: the key to new markets?", Industrial Robot: An International Journal, Vol. 43 Iss 3 pp. 258-263 <http://dx.doi.org/10.1108/IR-01-2016-0027>

Access to this document was granted through an Emerald subscription provided by emerald-srm:367394 []

For Authors

If you would like to write for this, or any other Emerald publication, then please use our Emerald for Authors service information about how to choose which publication to write for and submission guidelines are available for all. Please visit www.emeraldinsight.com/authors for more information.

About Emerald www.emeraldinsight.com

Emerald is a global publisher linking research and practice to the benefit of society. The company manages a portfolio of more than 290 journals and over 2,350 books and book series volumes, as well as providing an extensive range of online products and additional customer resources and services.

Emerald is both COUNTER 4 and TRANSFER compliant. The organization is a partner of the Committee on Publication Ethics (COPE) and also works with Portico and the LOCKSS initiative for digital archive preservation.

*Related content and download information correct at time of download.

Development of a dexterous continuum manipulator for exploration and inspection in confined spaces

Shuntao Liu

Chengdu Aviation Company, Chengdu, China

Zhixiong Yang and Zhijun Zhu

UM-SJTU Joint Institute, Shanghai Jiao Tong University, Shanghai, China

Liangliang Han

Institute of Aerospace System Engineering, Shanghai, China

Xiangyang Zhu

School of Mechanical Engineering, Shanghai Jiao Tong University, Shanghai, China, and

Kai Xu

Shanghai Jiao Tong University, Shanghai, China

Abstract

Purpose – Slim and dexterous manipulators with long reaches can perform various exploration and inspection tasks in confined spaces. This paper aims to present the development of such a dexterous continuum manipulator for potential applications in the aviation industry.

Design/methodology/approach – Benefiting from a newly conceived dual continuum mechanism and the improved actuation scheme, this paper proposes a design of a slim and dexterous continuum manipulator. Kinematics modeling, simulation-based dimension synthesis, structural constructions and system descriptions are elaborated.

Findings – Experimental validations show that the constructed prototype possesses the desired dexterity to navigate through confined spaces with its kinematics calibrated and actuation compensation implemented. The continuum manipulator with different deployed tools (e.g. graspers and welding guns) would be able to perform inspections and other tasks at remote locations in constrained environments.

Research limitations/implications – The current construction of the continuum manipulator possesses quite some friction inside its structure. The bending discrepancy caused by friction could accumulate to an obvious level. It is desired to further reduce the friction, even though the actuation compensation had been implemented.

Practical implications – The constructed continuum manipulator could perform inspection and other tasks in confined spaces, acting as an active multi-functional endoscopic platform. Such a device could greatly facilitate routine tasks in the aviation industry, such as guided assembling, inspection and maintenance.

Originality/value – The originality and values of this paper mainly lay on the design, modeling, construction and experimental validations of the slim and dexterous continuum manipulator for the desired mobility and functionality in confined spaces.

Keywords Inspection, Continuum manipulator, Continuum mechanism, Kinematics, Actuation compensation

Paper type Research paper

1. Introduction

Slim and dexterous manipulators with long reaches and exchangeable end effectors can perform various intra-cavity tasks in confined spaces, such as inspection, foreign objects removal, laser cutting, welding, manipulation and assembling. These appealing potential applications have led to a variety of research activities.

The research on slim and dexterous manipulators can be traced back to the 1960s when the Tensor Arm manipulator was developed (Anderson and Horn, 1970). Since then, many other dexterous manipulators have been developed (Paljug *et al.*, 1995; Wolf *et al.*, 2003; Hirose and Ma, 1991; Ma *et al.*,

The current issue and full text archive of this journal is available on Emerald Insight at: www.emeraldinsight.com/0143-991X.htm



Industrial Robot: An International Journal
43/3 (2016) 284–295
© Emerald Group Publishing Limited [ISSN 0143-991X]
[DOI 10.1108/IR-07-2015-0142]

This work was supported in part by the National Natural Science Foundation of China (Grant No. 51375295 and Grant No. 51435010), in part by the State Key Laboratory of Mechanical Systems and Vibration (Grant No. MSVZD201406 and Grant No. MSVZD201504), and in part by the Shanghai Rising-Star Program (Grant No. 14QA1402100).

Received 20 July 2015
Revised 27 September 2015
17 November 2015
7 January 2016
20 January 2016
Accepted 21 January 2016

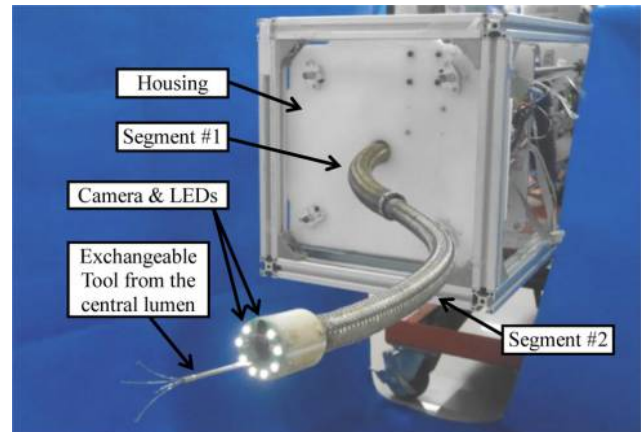
2002; Buckingham *et al.*, 2007; Buckingham and Graham, 2012; Suzumori *et al.*, 1991; McMahan *et al.*, 2006; Yang *et al.*, 2006; Rolf and Steil, 2012). Three main approaches were followed to design these dexterous manipulators as detailed below. The manipulators reviewed below are categorized from the construction and actuation point of view. Other categorization is certainly possible, such as according to the sizes and the intended applications:

- 1 A redundant manipulator is formed by several serially connected modules (e.g. the ones in Paljug *et al.*, 1995; Wolf *et al.*, 2003). Each module has one or two degrees of freedom (DoFs) with actuators integrated inside the module. The advantage is that one can easily construct a manipulator with the desired number of DoFs. But the main concern is that the number of the stacked modules is often limited, as the distal modules become overhead loads of the proximal ones. Because of this drawback, this approach was less adopted in recent developments.
- 2 Elastic materials (e.g. rubber and silicone) are used to form soft-bodied manipulators (Suzumori *et al.*, 1991; McMahan *et al.*, 2006; Yang *et al.*, 2006; Rolf and Steil, 2012). These soft-bodied manipulators are often driven by pneumatic or hydraulic pressure differentials. The advantages often include the relatively low cost for fabrication, light weight and intrinsic compliance. However, payload and positioning accuracy could be of concerns for these designs because of the discrepancy in modeling and the uncertainty in the material properties.
- 3 Cable actuation is used in the design of dexterous redundant manipulators (Hirose and Ma, 1991; Ma *et al.*, 2002; Buckingham *et al.*, 2007; Buckingham and Graham, 2012). Relatively high payload capability is an essential advantage for these designs. The main issue lies on the tension control of these actuation cables. When the manipulator is driven into a complex spatial shape, maintaining the tensions on the cables for accurate tip positioning can be quite challenging, given unavoidable cable elongation and friction. Although the challenges could be dealt benefitting from the advances in computational power, control algorithms and sensing technology, the cable-driven manipulators certainly do not rule out other design possibilities.

Other than a dexterous manipulator, active endoscopic cannulae could also be used to achieve exploration and inspection tasks in confined spaces. These endoscopic cannulae usually possess an underactuated construction and lockable components for them to navigate into complex cavities for remote tasks (Degani *et al.*, 2007; Yagi *et al.*, 2006; Zuo *et al.*, 2008; Loeve *et al.*, 2010, 2012; Kim *et al.*, 2013). It is usually a lengthy process for these cannulae to considerably change their pose from one to another because of their underactuated construction. The dexterity of these cannulae is usually not enough to explore a complex cavity.

Inspired by the continuum robots with multiple backbones and push-pull actuation as in the studies by Simaan *et al.* (2009), Xu and Simaan (2010b), Zhao *et al.* (2013), Rone and Ben-Tzvi (2014) and Xu *et al.* (2015), this paper proposes to design a slim and dexterous continuum manipulator as shown in Figure 1. The manipulator consists of two continuum segments. Each continuum segment possesses three DoFs. A

Figure 1 A dexterous continuum manipulator for exploration and inspection



camera unit with integrated LEDs for illumination is installed at the distal tip with a lumen in the manipulator body for passing different tools for various tasks.

As explained in later sections of this paper, the continuum segments of the manipulator are actuated by pushing and pulling their backbones, utilizing the benefits of a newly proposed dual continuum mechanism concept. The backbones are made from super-elastic nitinol rods which could undertake both compressive and stretching loads. All the actuators are located at the proximal end of the manipulator and they work collectively to drive the segments. And the segments are bent because of compatible deformations of all the structural members when the backbones are pulled and pushed. Tensions on the backbones need not be deliberately maintained. The Young's modulus of the nitinol is considerably higher than that of the non-metal elastic materials such as rubber and silicone. Using nitinol to construct the continuum segments could lead to better payload capabilities and higher positioning accuracy, with proper motion calibrations implemented. With the structure synthesized using the kinematics model, the continuum manipulator is expected to navigate through a mockup environment to perform inspections or manipulations at remote locations in a deep cavity.

Originality and contributions of this paper mainly lay on the design, modeling, construction and experimental validations of the slim and dexterous continuum manipulator for the desired mobility and functionality in confined spaces. Although the very first design concept of this type of continuum manipulator is not proposed by this paper, this paper presents the first attempt to construct such a continuum manipulator at the current size and length-over-diameter ratio, which is by no means a trivial task. Many design considerations, which are elaborated in later sections, contributed to this successful implementation. More than just building a prototype, this paper further demonstrates that by implementing the presented construction, such a relatively big continuum manipulator could still be described and controlled using existing simple and effective kinematics formulation that enables tele-operated robotic surgery as in (Simaan *et al.*, 2009; Xu and Simaan, 2010b; Zhao *et al.*, 2013; Xu *et al.*, 2015). The results could be truly appealing to industry, potentially avoiding sophisticated nonlinear mechanics for the kinematics and dynamics formulations of a continuum manipulator as in recent studies (Camarillo *et al.*, 2008; Rone

and Ben-Tzvi, 2014; Rucker and Webster, 2011). The constructed prototype showed that routine tasks in the aviation industry, such as guided assembling, inspection and maintenance, could be done much more efficiently and conveniently with this dexterous continuum manipulator. The applicability of continuum manipulator technology seems promising in the industrial settings similar to the presented scenarios.

This paper is organized as follows. Section 2 presents the design goals. Kinematics-based structure synthesis and simulations of the manipulator is presented in Section 3. Section 4 describes the system construction and various system components in detail. Motion calibration, actuation compensation and navigation demonstrations are reported in Section 5. Conclusions and future works are summarized in Section 6.

2. Design goals and overview

It is often troublesome to perform many routine tasks in the aviation industry, such as inspection, foreign objects removal, structure modification (e.g. cutting and welding), manipulation and assembling in confined spaces. To better facilitate these routine tasks, a slim and dexterous manipulator acting as an endoscopic tooling platform is in great need. The desired functionalities of such a manipulator could be listed as follows:

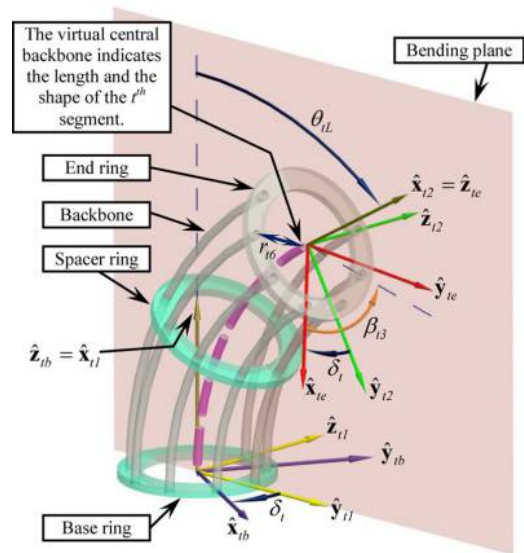
- the manipulator should be dexterous enough to reach various remote locations in a deep cavity;
- the manipulator should be slim enough to navigate through complex internal structures and/or avoid obstacles in confined spaces;
- a camera head with integrated illumination is installed at the tip of the manipulator for inspections and visual guidance;
- at least one lumen is available inside the manipulator for tool delivery and/or object retrieval; and
- various tools (e.g. graspers, welding guns and laser cutters) could be delivered to the distal site through the lumen inside the manipulator for various tasks.

A continuum manipulator as shown in Figure 1 was developed to address the aforementioned needs. The manipulator with a total reach of 1,000 mm consists of two continuum segments with outer diameters of 19 and 27.5 mm. Each segment that is also depicted in Figure 2 has three DoFs (2-DoF bending plus 1-DoF lengthening/shortening). Bent shapes of the segments could be approximated by circular arcs according to the theoretic and experimental studies (Xu and Simaan, 2010a, 2008). A camera head with integrated LEDs are installed at the tip of this dexterous manipulator for illumination and visual guidance. A $\varnothing 10$ -mm lumen is available inside the manipulator for the insertion of additional exchangeable tools for different tasks.

3. Kinematics and structural synthesis

The proposed continuum manipulator mainly consists of two segments. The schematic of each continuum segment is depicted in Figure 2. Each segment consists of a base ring, several spacers, an end ring and several backbones. The backbones are all made from super-elastic nitinol rods. Pushing and/or pulling these backbones drives one segment: differentially pushing and pulling realizes a 2-DoF bending, whereas synchronously pushing or

Figure 2 Nomenclature and coordinates of the t^{th} segment



pulling realizes a 1-DoF lengthening/shortening of each segment. The spacer rings are distributed evenly along one segment to prevent the buckling of the backbones.

With nomenclature and coordinates defined in Section 3.1, the kinematics is derived in Section 3.2 and 3.3. Then structure synthesis and simulations are reported in Section 3.4.

3.1 Nomenclatures and coordinates

The continuum manipulator in Figure 1 consists of two segments. The t^{th} segment ($t = 1, 2$) is shown in Figure 2, whereas the nomenclatures are defined in Table I. Coordinate systems of the t^{th} segment are defined as below:

- *Base Ring Coordinate* $\{tb\} \equiv \{\hat{x}_{tb}, \hat{y}_{tb}, \hat{z}_{tb}\}$: It is attached to the base ring of the t^{th} segment. The XY plane is aligned with the base ring with its origin at the center. \hat{x}_{tb} points

Table I Nomenclature used in this paper

i	Index of the backbones, $i = 1, 2, \dots, m$
t	Index of the segments $t = 1, 2$; numbering of the segments always precedes the backbones
r_{ti}	Radius of the pitch circle defining the positions of the i^{th} backbone in all the rings of the t^{th} segment. r_{t6} is indicated in Figure 2
β_{ti}	Division angle of the i^{th} backbone along the circumference of the pitch circle. β_{t3} is indicated in Figure 2
L_t, L_{ti}	Lengths of the virtual central backbone and the i^{th} backbone of the t^{th} segment
$\theta_t(s)$	The angle of the tangent to the virtual central backbone in the bending plane. $\theta_t(L_t)$ is denoted by θ_{tL}
δ_{ti}	For the t^{th} segment, a right-handed rotation angle from \hat{y}_{ti} about \hat{z}_{tb} to a ray passing through the i^{th} backbone
δ_t	$\delta_t \equiv \delta_{t1}$ and $\delta_{ti} = \delta_t + \beta_{ti}$
ψ_t	$\psi_t = [\theta_{tL}, \delta_t, L_t]^T$ is a configuration vector which defines the status of the t^{th} segment
1R_2	Coordinate transformation matrix Frame 2 to Frame 1
${}^{tb}p_i(s)$	Position vector of a point along the central backbone in $\{tb\}$. ${}^{tb}p_i(L_t)$ is the tip position designated by ${}^{tb}p_{tL}$

from the center to the first backbone. The backbones are numbered according to the definition of δ_i .

- *Bending Plane Coordinate-1* $\{t1\} \equiv \{\hat{x}_{t1}, \hat{y}_{t1}, \hat{z}_{t1}\}$: It shares its origin with $\{tb\}$ and has the t^{th} segment bending in its XY plane.
- *Bending Plane Coordinate-2* $\{t2\} \equiv \{\hat{x}_{t2}, \hat{y}_{t2}, \hat{z}_{t2}\}$: It is obtained from $\{t1\}$ by a rotation about \hat{z}_{t1} such that \hat{x}_{t2} becomes backbone tangent at the end ring. Origin of $\{t2\}$ is at center of the end ring.
- *End Ring Coordinate* $\{te\} \equiv \{\hat{x}_{te}, \hat{y}_{te}, \hat{z}_{te}\}$: It is fixed to the end ring. \hat{x}_{te} points from the end ring center to the first backbone and \hat{z}_{te} is normal to the end ring.

When the $(t + 1)^{th}$ segment is stacked on top of the t^{th} segment, $\{te\}$ coincides with $\{(t + 1)b\}$.

3.2 Kinematics of the t^{th} segment

Thorough derivation of the kinematics of one continuum segment can be found in few studies (Xu and Simaan, 2008, 2010b; Jones and Walker, 2006; Webster and Jones, 2010; Dupont et al., 2010; Bai, 2014). Related entities are summarized here. Kinematics of the t^{th} segment will be used to assemble the kinematics of the entire manipulator as in Section 3.3. It will also be used for the structural synthesis as in Section 3.4.

The length and the shape of the t^{th} segment is specified by the virtual central backbone and parameterized by the configuration vector $\psi_t = [\theta_{tL} \ \delta_t \ L_t]^T$. It has been shown via analytical derivations and experimentations that the t^{th} segment bends into a shape that is close to a circular arc (Xu and Simaan, 2008, 2010a).

This modeling approximation of circular bending leads to two sets of derivations. In the first set of derivations, the virtual central backbone is close to a circular arc. Center of the end ring of the t^{th} segment is hence as follows:

$${}^{tb}\mathbf{p}_{tL} = \frac{L_t}{\theta_{tL}} \begin{bmatrix} \cos \delta_t (1 - \cos \theta_{tL}) \\ \sin \delta_t (\cos \theta_{tL} - 1) \\ \sin \theta_{tL} \end{bmatrix} \quad (1)$$

Where ${}^{tb}\mathbf{p}_{tL} = [0 \ 0 \ L_t]^T$ when $\theta_{tL} = 0$.

Coordinate transformation matrix ${}^{tb}\mathbf{R}_{te}$ relates $\{te\}$ and $\{tb\}$:

$${}^{tb}\mathbf{R}_{te} = {}^{tb}\mathbf{R}_{t1} {}^{t1}\mathbf{R}_{t2} {}^{t2}\mathbf{R}_{te} \quad (2)$$

Where ${}^{tb}\mathbf{R}_{t1} = \begin{bmatrix} 0 & \cos \delta_t & \sin \delta_t \\ 0 & -\sin \delta_t & \cos \delta_t \\ 1 & 0 & 0 \end{bmatrix}$,

$${}^{t1}\mathbf{R}_{t2} = \begin{bmatrix} \cos \theta_{tL} & -\sin \theta_{tL} & 0 \\ \sin \theta_{tL} & \cos \theta_{tL} & 0 \\ 0 & 0 & 1 \end{bmatrix}$$

and ${}^{t2}\mathbf{R}_{te} = \begin{bmatrix} 0 & 0 & 1 \\ \cos \delta_t & -\sin \delta_t & 0 \\ \sin \delta_t & \cos \delta_t & 0 \end{bmatrix}$.

In the second set of derivations, all the backbones are bent into circular arcs in planes parallel to the bending plane. The projection of the i^{th} backbone on the bending plane has the same length as the backbone itself. The projection is offset from the virtual central backbone within the bending plane. The lengths of the virtual central backbone and the i^{th} backbone are related as in equation (3). Derivations details

could refer to those in the studies by Xu and Simaan (2008) and Xu and Simaan (2010b):

$$L_{ii} = L_t - r_{ii} \theta_{tL} \cos(\delta_t + \beta_{ii}) \quad (3)$$

Pushing and pulling of the backbones as actuation should refer to equation (3) to bend the t^{th} segment for the position and orientation of the end ring as in equations (1) and (2). Arrangements of the backbones, which are specified by r_{ii} and β_{ii} , could be arbitrary as long as they are all actuated according to equation (3).

3.3 Kinematics of the continuum manipulator

In the manipulator as shown in Figure 1, Segment 1 is extended from the housing to realize the length change, while Segment 2 is extended from the central lumen of Segment 1.

Shape of the extruded portion of Segment 1 would be described by the kinematics model in Section 3.2, as the portion of Segment 1 which is inside the housing is assumed not to be bent or deformed. When Segment 2 is extended from the central lumen of the Segment 1, similarly, only the extruded portion would be bent. The extruded portion would be treated as the second segment which is stacked on top of the Segment 1. The portion of the Segment 2 which is inside the Segment 1 will assume the shape of the Segment 1. This portion is assumed not to affect the shape of the extruded portion of the Segment 2.

When the Segment 2 is extended from the Segment 1, $\{1e\}$ of the Segment 1 coincides with $\{2b\}$ of the Segment 2, as twisting of the two segments is neglected. A configuration vector $\xi = [\psi_2^T \ \psi_1^T]^T$ parameterizes the manipulator. The tip position of the end effector in $\{1b\}$ can be written as follows:

$${}^{1b}\mathbf{p}_g = {}^{1b}\mathbf{p}_{1L} + {}^{1b}\mathbf{R}_{2b} ({}^{2b}\mathbf{p}_{2L} + {}^{2b}\mathbf{R}_{2e} {}^{2e}\mathbf{p}_g) \quad (4)$$

Where ${}^{1b}\mathbf{p}_{1L}$ and ${}^{2b}\mathbf{p}_{2L}$ can be obtained from equation (1); and ${}^{2e}\mathbf{p}_g$ is the tip position of the end effector in $\{2e\}$.

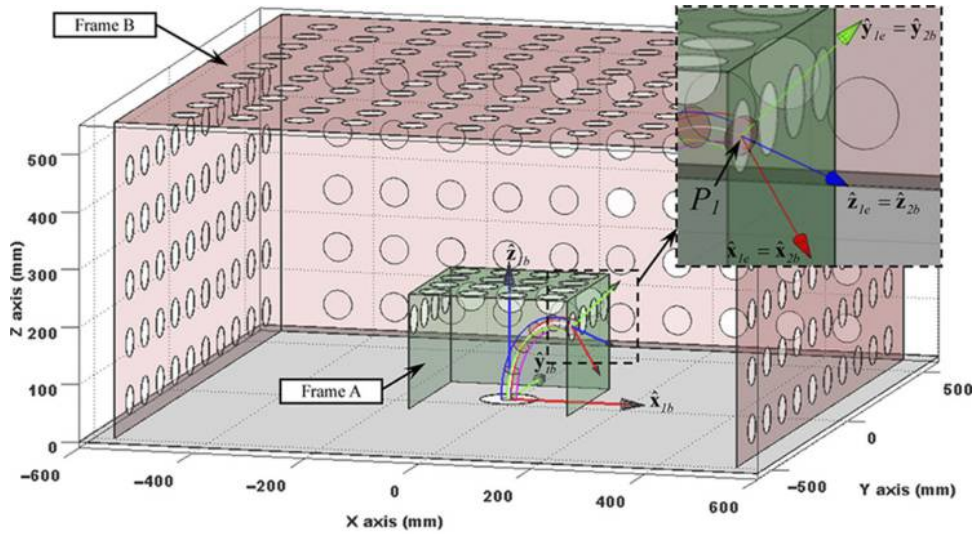
3.4 Structural synthesis

The manipulator is designed to perform remote tasks in the mockup cavity that is shown in Figure 3. The cavity is abstracted from a specific structure of an aircraft's subsystem. The continuum manipulator is expected to enter the cavity at the $[0 \ 0 \ 0]^T$ point and navigate through the holes in the inner Frame A to reach every hole in the outer Frame B. The distance between the rows and columns of the holes is 70 mm in Frame A and 100 mm in Frame B. The dimensions of the inner frame A is 280 mm by 280 mm by 200 mm, while the dimensions of the outer frame B are 1,100 mm by 1100 mm by 550 mm.

The structure synthesis is performed to generate proper parameters of the manipulator so that the holes in the B frame could all be reached. The synthesis is performed in an enumerative manner in this paper.

It was first assumed that the holes in the Frame A will be reached by the Segment 1, while the holes in the Frame B will be reached by the Segment 2. Then when the *PI* point is reached by the Segment 1 as shown in Figure 3(a), the desired configuration of the Segment 1 $\psi_1 = [\theta_{1L} \ \delta_1 \ L_1]^T$ can be solved by the following equation:

Figure 3 The mockup cavity for the design of the manipulator



Note: Frame A is the inner frame while frame B is the outer frame of the cavity

$${}^{1b}\mathbf{p}_{1L} = \frac{L_1}{\theta_{1L}} \begin{bmatrix} \cos \delta_1 (1 - \cos \theta_{1L}) \\ \sin \delta_1 (\cos \theta_{1L} - 1) \\ \sin \theta_{1L} \end{bmatrix} = \begin{bmatrix} P_{1x} \\ P_{1y} \\ P_{1z} \end{bmatrix} \quad (5)$$

Where ${}^{1b}[P_{1x} \ P_{1y} \ P_{1z}]$ is the coordinates of $P1$ in $\{1b\}$.

Then when the $P2$ point is to be reached by the Segment 2, the desired configuration $\psi_2 = [\theta_{2L} \ \delta_2 \ L_2]^T$ can be solved from equation (6):

$${}^{2b}\mathbf{p}_{2L} = \frac{L_2}{\theta_{2L}} \begin{bmatrix} \cos \delta_2 (1 - \cos \theta_{2L}) \\ \sin \delta_2 (\cos \theta_{2L} - 1) \\ \sin \theta_{2L} \end{bmatrix} = \begin{bmatrix} P_{2x} \\ P_{2y} \\ P_{2z} \end{bmatrix} \quad (6)$$

Where ${}^{2b}[P_{2x} \ P_{2y} \ P_{2z}]^T$ is the coordinates of $P2$ in $\{2b\}$ and it could be obtained by equation (7):

$$\begin{bmatrix} P_{2x} \\ P_{2y} \\ P_{2z} \end{bmatrix} = ({}^{1b}\mathbf{R}_{2b})^{-1} \left(\begin{bmatrix} P_{2x} \\ P_{2y} \\ P_{2z} \end{bmatrix} - {}^{1b}\mathbf{p}_{1L} \right) \quad (7)$$

Where ${}^{1b}[P_{2x} \ P_{2y} \ P_{2z}]^T$ is the coordinates of P_2 in $\{1b\}$ and it is known once the cavity is constructed; ${}^{1b}\mathbf{R}_{2b}$ is identical to ${}^{1b}\mathbf{R}_{1e}$, as $\{1e\}$ coincides with $\{2b\}$, as twisting of the two segments is neglected.

It is preferred to find out an optimized structure of the continuum manipulator so that with minimal values of L_1 and L_2 , all the holes in the Frame B could be reached by the manipulator. The optimization is conducted in an enumerative manner as follows:

- To reach a certain hole in the Frame B, all the possible configurations $\xi = [\psi_2^T \ \psi_1^T]^T$ of the manipulator are generated by navigating different holes in the Frame A to reach the specific hole in the Frame B. The manipulator configuration can be obtained solving equations (5) and (6).
- A configuration of the manipulator is invalidated if the 1st or the Segment 2 exceeds a 90° bending. Then

among all the possible configurations, the one with the smallest $L = L_1 + L_2$ value is selected.

- All the holes in the Frame B are tested using the Steps 1 and 2. N configurations of the manipulator are generated. N is the number of holes in the Frame B. Among the N configurations, the lengths of Segments 1 and the 2 are selected as the longest L_1 and L_2 values, respectively, to ensure all the holes in the Frame B could be reached.

A few configurations of the manipulator are shown in Figure 4, reaching various holes in the Frame B. The configurations $\xi = [\psi_2^T \ \psi_1^T]^T$ are listed below:

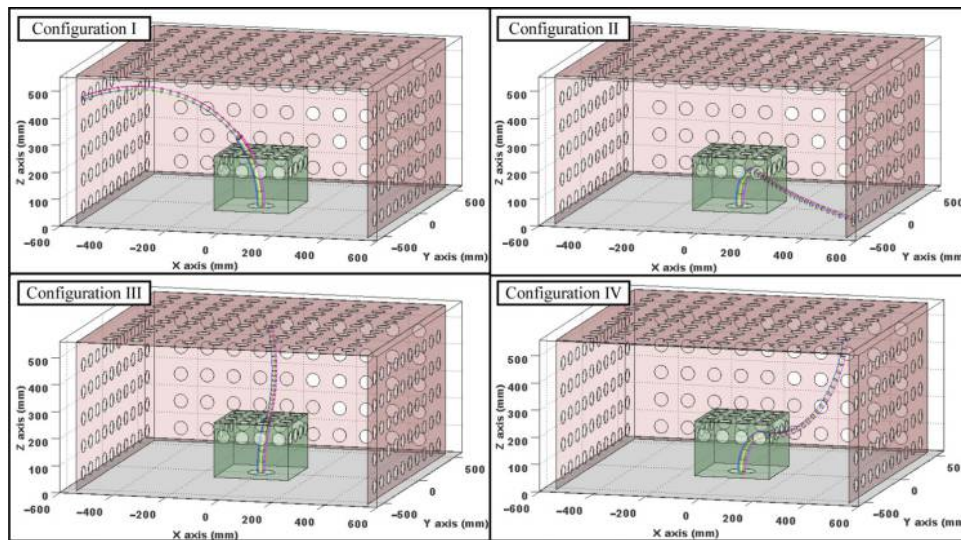
- $\xi_I = [0.680 \text{ rad} \ 2.356 \text{ rad} \ 281.2 \text{ mm} \ 1.201 \text{ rad} \ 2.551 \text{ rad} \ 688.3 \text{ mm}]$
- $\xi_{II} = [1.564 \text{ rad} \ 0.921 \text{ rad} \ 247.2 \text{ mm} \ 0.716 \text{ rad} \ -0.058 \text{ rad} \ 581.8 \text{ mm}]$
- $\xi_{III} = [0.485 \text{ rad} \ 0.785 \text{ rad} \ 208.1 \text{ mm} \ 0.849 \text{ rad} \ -2.356 \text{ rad} \ 361.4 \text{ mm}]$
- $\xi_{IV} = [1.538 \text{ rad} \ 0.644 \text{ rad} \ 238.5 \text{ mm} \ 1.570 \text{ rad} \ -2.322 \text{ rad} \ 605.7 \text{ mm}]$

Simulations were carried out to verify that the holes in Frame B could all be reached. Rounding the obtained L_1 and L_2 values, the parameters of the manipulation are decided as in Table II.

4. System construction and component descriptions

With the manipulator structure synthesized in Section 3, this section elaborates the construction of the manipulator so that the desired motions could be realized.

The structure of this continuum manipulator is inspired by the miniature manipulator adopted in the surgical robotic systems as in few studies (Simaan et al., 2009; Xu and Simaan, 2010b; Zhao et al., 2013; Xu et al., 2015). But the continuum manipulator to be constructed here is substantially bigger. Specific challenges and design

Figure 4 Configurations of the manipulator during exploration of the mockup cavity

Note: Configuration I to IV show typical poses of the manipulator

Table II Structure parameters of the distal segments of the manipulator

$\theta_{iL} \in [0, \pi/2]$	$\delta_i \in [-\pi, \pi]$	$L_1 \in [0, 300\text{mm}]$
$r_{1i} = 11.75\text{mm}$	$r_{2i} = 7.5\text{mm}$	$L_2 \in [0, 700\text{mm}]$

considerations for the construction of the continuum manipulator are elaborated in Section 4.1.

4.1 Continuum segments

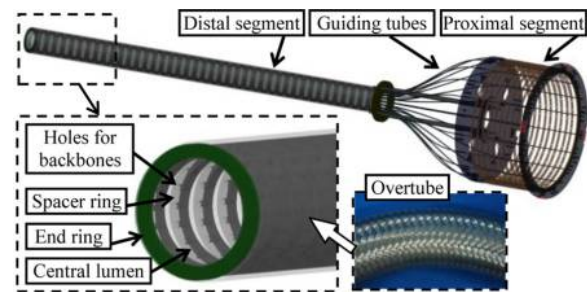
Two continuum segments are used to form the manipulator as shown in Figure 1, while the kinematics of one segment is shown in Figure 2. The segment in its actual size is thin and long. Several challenges are encountered during the construction of the segments and the manipulator:

4.1.1 Effects of gravity and the selection of backbones

As the segments to be made are relatively large, gravity might affect the bending shapes. According to the elasticity analysis in the study by Xu and Simaan (2008), the nitinol backbones should be thick enough so that the elastic potential energy outweighs the gravitational potential energy during bending. In this way, effects of gravity might be reduced. Following the analysis, the diameter of the backbones should ideally be more than 2.0 mm. Because of the considerations about the central lumen elaborated below, the backbone diameter is eventually selected to be 1.0 mm.

4.1.2 Central lumen and the dual continuum mechanism

The distal tip of the Segment 1 is shown in the inset of Figure 5. A lumen in the center should be spared so that other segments or exchangeable tools could be inserted. It is desired the lumen could be as big as possible for a given outer diameter of the segment. Using a thick backbone would increase the wall thickness of the segment, hence reducing the size of the central lumen. To reduce the wall thickness while maintaining a high value of the elastic potential energy, 20 Ø1 mm backbones are used in the Segment 1. In the analysis in the study by Xu and

Figure 5 Design of the Segment 1 using the concept of dual continuum mechanism

Simaan (2008), the elastic potential energy comes from only three backbones. It should be noted that the use of 20 Ø1 mm backbones is just one possible design scheme. Depending on the availability of the nitinol materials, other combinations of the number and the diameters of the backbones could be adopted, as long as the elastic potential energy outweighs the gravitational potential energy.

Simultaneous push–pull actuation of the backbones bends the segment. The actuated lengths of the backbones depend on three variables (θ_{iL} , δ_i and L_i) according to equation (3). Obviously it is not desired to use 20 motors to drive the 20 backbones in the Segment 1, as the 20 lengths depend on three variables. The concept of the dual continuum mechanism is hence adopted as shown in Figure 5. The concept was originally introduced in (Xu et al., 2014, 2015). The Segment 1 in Figure 5 actually consists of the 1st distal segment, the 1st proximal segment and a set of rigid guiding tubes. In all, 20 Ø-1mm super-elastic nitinol rods, as the segments' backbones, are routed from the distal segment to the proximal segment through the guiding tubes. Both segments have a structure similar to the one shown in Figure 2. The arrangement of the backbones is

similar and scaled so that bending of the proximal segment bends the distal segment in the opposite direction.

The actuation assembly presented in Section 4.2 would bend the proximal segment so as to bend the distal segment. As the distal segment is essentially actuated by the proximal segment, the actuation of each individual backbone now does not depend on how many backbones are arranged in the dual continuum mechanism.

4.1.3 Segments' overtube

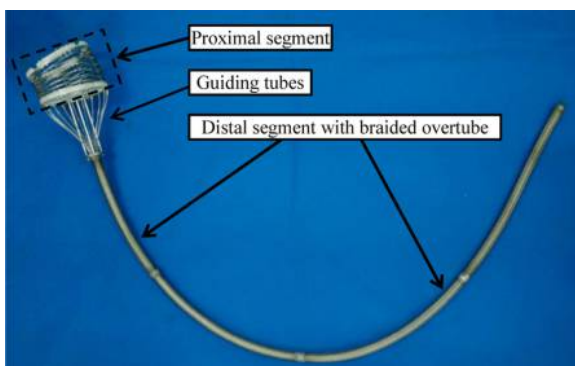
Torsional rigidity of the segment's structure as in Figure 2 is relatively low. A braided stainless steel overtube shown in the inset of Figure 5 is hence used to cover and reinforce each distal segment. These stainless steel over tubes can enhance the torsional rigidity of the distal segments without compromising their bending capabilities. This enhancement is essential for increasing the loading capability according to the experimental results in the studies by Zhao *et al.* (2013) and Xu *et al.*, (2015); and validating the no-twist modeling assumptions in Sections 3.2 and 3.3. The over tubes also provide smooth surfaces to facilitate the insertion of one segment into one another.

4.1.4 Friction

There is friction between the backbones and the holes in the spacer rings. The friction would affect the segments' bending shapes and should be minimized. Polytetrafluoroethylene (PTFE) is hence used to make the spacer rings as shown in Figures 2 and 5. The distance between two adjacent spacer rings is about 15 mm. A spacer ring made from stainless steel is arranged every 10 PTFE spacer rings. The stainless steel ring is soldered to the overtube to maintain the torsional rigidity of the segment.

Following the aforementioned considerations, the continuum segments are designed and constructed, with the Segment 1 shown in Figure 5 and the Segment 2 shown in Figure 6. Both segments utilize the concept of the dual continuum mechanism, and include the distal segments and the proximal segments. As shown in Figures 5 and 6, bending of the proximal segments would bend the distal segments in the opposite directions. The 1st distal segment in Figure 5 has an outer diameter of 27.5 mm and an inner diameter of 21.5 mm, while the 2nd distal segment in Figure 6 has an outer diameter of 19 mm and an inner diameter of 13 mm. The 2nd distal segment is inserted into the 1st distal segment. And the

Figure 6 Construction of the Segment 2 using the concept of dual continuum mechanism



vision unit presented in Section 4.3 is then assembled on the distal tip of the Segment 2 to entirely form the continuum manipulator as shown in Figure 1. Exchangeable tools can be inserted through the central lumen to perform various tasks at remote locations. The 2nd distal segment could be completely housed inside the Segment 1. When it is pushed out and bent, the effective length of the Segment 2 varies between 0 and 700 mm. The 1st distal segment can be housed inside manipulator housing and can be pushed out to realize an effective length between 0 and 300 mm. The structural parameters of the manipulator are listed in Table II.

The two proximal segments of Segments 1 and 2 are identical with outer diameters of 135 mm and inner diameters of 125 mm. In all, 20 backbones are used in both Segments 1 and 2. The backbones are super-elastic nitinol rods with diameters of 1.0 mm. The guiding tubes for passing the backbones have outer diameters of 1.6 mm and inner diameters of 1.2 mm. The two ends of each guiding tube are soldered to the base rings of the corresponding distal and proximal segments so that motions of the proximal segment could be faithfully transmitted to the distal segment.

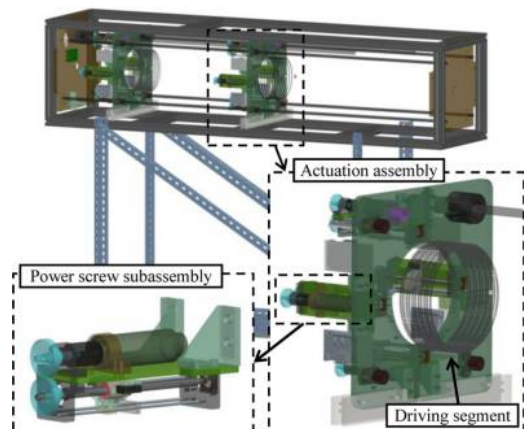
After motion calibration and actuation compensation as presented in Section 5.1, the manipulator had shown satisfactory positioning accuracy. This demonstrates the effectiveness of the approaches and considerations for the construction of these continuum segments.

4.2 Actuation unit

The actuation unit in Figure 7 consists of two identical actuation assemblies. Each actuation assembly includes a driving segment, and four power screw subassemblies. The proximal Segments 1 and 2 in Figures 5 and 6 can be assembled into driving segment of each actuation assembly such that bending of the driving segment would bend the assembled proximal segments so as to drive the corresponding distal segments.

The structure of each driving segment is similar to the one shown in Figure 2. Four actuation backbones are attached to the end ring and they are arranged 90° apart along a circle with a diameter of 140 mm. The backbones are pulled or pushed to bend the driving segment by the power screw subassemblies according to the actuation kinematics as in equation (3). Each driving segment has an outer diameter of 145 mm, an inner

Figure 7 Actuation unit with two actuation assemblies



diameter of 136 mm and a matching length of the proximal segments.

The ball screw in the power screw subassembly has a diameter of 6 mm, a lead of 2 mm and an effective travel of 90 mm. The driving segment is bent by pushing and pulling the actuation backbones. When the proximal segment is assembled into the driving segment, the proximal segment is assumed to have the same amount of bending as the driving segment. Then the driving segment is bent together with the proximal segment to drive the distal segment, realizing a 2-DoF bending of the distal segment, no matter how many backbones are arranged in the continuum manipulator.

Although partially constrained in the housing, only the extruded part of the distal segment could be bent. This is equivalent to actively changing the effective length of the distal segment. After the proximal segments are assembled to the driving segments of the actuation assembly, the actuation assemblies are translated back and forth to realize the length change of the 1st and the 2nd distal segments. The length changing ranges are listed in Table II. Sliding bushings are used to guide the translations of the actuation assemblies. The translations are realized using motorized $\varnothing 12$ -mm lead screws with a lead of 2-mm.

Each segment hence uses five servomotors for actuation (four for bending and one for translation). In total, ten servomotors are used. It should be noted that the bending of one segment theoretically only needs two servomotors, as the bending motion is a 2-DoF one. The use of four servomotors to push and pull the backbones in the driving segment is because of the difficulty in realizing the coupled push-pull motions of the two backbones that are 180° apart.

WXY10 linear potentiometers with a travel of 800 mm are used to measure the absolute translation between the adjacent actuation assemblies. Two KTL linear potentiometers with a travel of 100 mm are used to measure the absolute amount of pushing and pulling of the backbones in the power screw subassembly.

4.3 Integrated vision with illumination

The vision unit with integrated illumination is installed at the tip of the manipulator to provide visual guidance during inspection and task execution, as shown in Figure 8.

The MO-B3506 camera chip (Misumi Inc.) with a diameter of 7.7 mm, a length of 10.5 mm and a resolution of 640×480 is used in the vision unit. The chips' original wires were

Figure 8 Integrated vision unit with LEDs

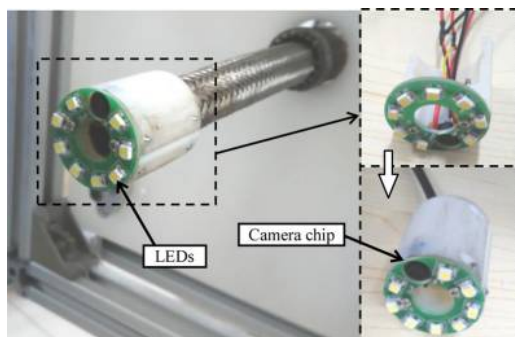
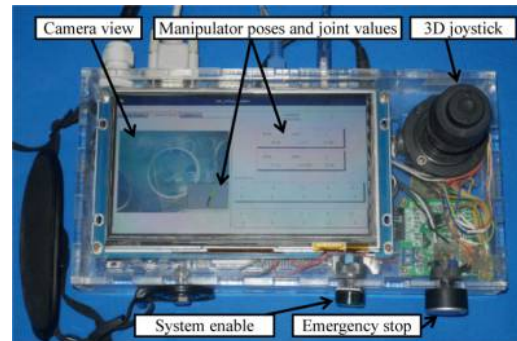


Figure 9 Central controller and control panel of the manipulator



extended to allow the transmission of the video signal to the control panel, shown in Figure 9.

A ring-shaped printed circuit board was customized for the mounting of eight LEDs for illumination. Each of these LEDs has a power rating of 0.06 W and a rated voltage of 3.0 V. Continuous lighting of these LEDs does not cause a heating problem. The steady status temperature is about 28°C when the vision unit is placed in an indoor environment under a room temperature of 20°C with no active ventilation.

4.4 Control infrastructure and user interface

In each actuation assembly, four servomotors are used to bend the driving segment and one is used for translation. In total, ten servomotors are used in the actuation unit to drive the manipulator. The motors are the DCX22L motors from Maxon Inc with the GPX-22 gearheads (gear ratio of 21:1) and the ENX16 encoders (512 Counts per Turn). Ten Maxon EPOS2 24/2 digital controllers are used to control the servomotors. Desired positions are transmitted from the central controller to the EPOS2 controllers via CAN buses in a broadcasting mode every 2ms.

The central controller in Figure 9 is a Cortex-A8 embedded system (TQ-AM335X from Guangzhou Embedsky Computer Technology Co., Ltd). It is equipped with a 7-inch Capacitive Touch Screen, a 1 GHz CPU and two channels of CAN transceivers. Each CAN channel communicates with five EPOS2 controllers.

A user operates a 3D joystick to control the motion of each segment, as each segment has three DoFs. The initial scheme for user inputs is to use the 3D joystick to control the θ_{iL} , δ_i and L_i values of each segment one by one. The button on the top of the joystick is used to select which segment to control. The segment which is not actively controlled will remain its current configuration. Modifications of the user input scheme will be proposed once this method is found to be counterintuitive to a user.

The control panel also provides other basic functions, such as system enable, emergency stop and manipulator homing. View of the onboard camera is transmitted and displayed on the control panel for the visual guidance. To better assist the user for the control of the manipulator, a simulated rendering of the current manipulator pose is also displayed around the corner of the camera view. Joint values of the manipulator are displayed next to the camera view.

5. Experimental validations

With the dexterous continuum manipulator constructed, two sets of experiments were carried out to characterize its specifications and demonstrate its capabilities.

5.1 Calibration and actuation compensation

It has been shown that there often exists a shape discrepancy between the actual shape and the assumed ideal shape of one continuum segment (Xu and Simaan, 2006, 2010a). Hence, actuation compensation is necessary to deform the manipulation into the desired shapes for better execution of the intended tasks.

The compensation was conducted for both segments in a similar manner. The experimental setup is shown in Figure 10 and the procedure is elaborated here for Segment 2 as follows:

- Segment 2 was driven to a desired configuration that was specified by $\psi_t = [\theta_{tL}, \delta_t, L_t]^T$.
- Three markers are attached to the tip and the base ring of Segment 2, as shown in Figure 10. An optical tracker (Micron Tracker SX60, Claron Technology Inc.) tracked the markers during the bending calibration. The tip's actual orientation and position was calculated with respect to the base ring and the results were compared to the tip's desired orientation and position.
- The tracker's position was adjusted to maintain the measurement accuracy with the tip marker changing its orientation during the bending calibration, according to the compensation process in the study by Xu et al. (2015).

The representative bending errors on θ_{tL} are plotted in Figure 11, when δ_t was commanded between 0° and 360° with θ_{tL} commanded at 45° and L_t commanded at 300 mm. Bending

Figure 10 Experimental setup for bending calibration

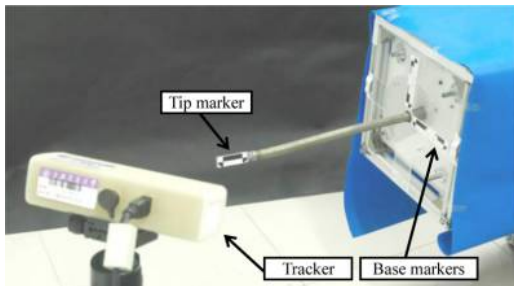
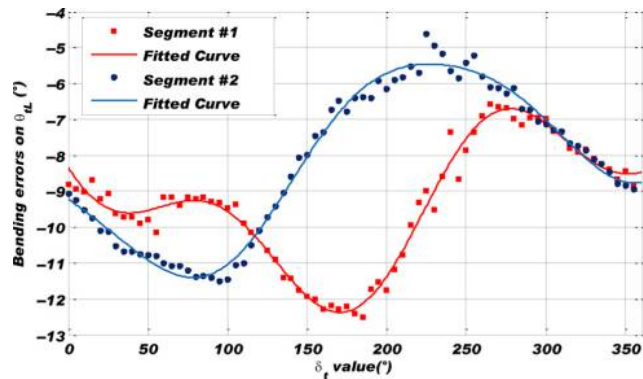


Figure 11 Bending errors on θ_{tL} of Segments 1 and 2



errors on θ_{1L} and θ_{2L} are recorded in two separate sets of experiments. These errors were fitted using the following function:

$$e_{tL} = \sum_{k=1}^3 [a_{tk} \sin(b_{tk} \delta_t + c_{tk})], \quad t = 1 \text{ or } 2 \quad (8)$$

With the coefficients a_{tk} , b_{tk} and c_{tk} obtained via curving fitting, the actuation compensation for Segments 1 and 2 could be expressed as in equation (9). The actuation compensation is implemented using the measurements with θ_{tL} set to 45° . This is because the bending errors, when the segments are bent to different angles, are approximately proportional to the errors when the segments are bent to 45° :

$$\tilde{\theta}_{tL} = \theta_{tL} + \frac{\theta_{tL}}{\pi/4} e_{tL} \frac{\pi}{180^\circ}, \quad t = 1 \text{ or } 2 \quad (9)$$

Where $\tilde{\theta}_{tL}$ is the commanded value for a desired θ_{tL} bending. e_{tL} has a unit of degree and it shall be converted into radian.

Because of redundant arrangement of the backbones in the segments, the errors on δ_t were between $\pm 1.5^\circ$. It was also found that errors on the segment lengths L_t were always between ± 1.2 mm. These results were considered acceptable and the compensations on δ_t and L_t are hence not implemented.

Using the compensated command values $\tilde{\theta}_{tL}$, the bending discrepancy can be reduced. As shown in Figure 12, the bending errors on θ_{tL} are now mostly between $\pm 2^\circ$. The biggest error is about 3.8° . Even with the actuation compensation, essentially the continuum manipulator is still in an open-loop control mode. The servomotors only close the control loop at the motor shafts with the motor encodes. The manipulator tip orientation and position depend on its deformed shape and transmissions from the motor shafts to the backbone translations. With the uncertainty on the repeatability of the manipulator's internal deformed structure and backlashes in the transmission, it could be quite challenging to further reduce these errors without an accurate feedback of the distal orientation. In the particular application of the cavity exploration shown in Section 5.2, the accuracy is considered enough, as the visual guidance is supplied using the integrated distal camera. An operator could always

Figure 12 Bending errors of Segments 1 and 2 after compensation

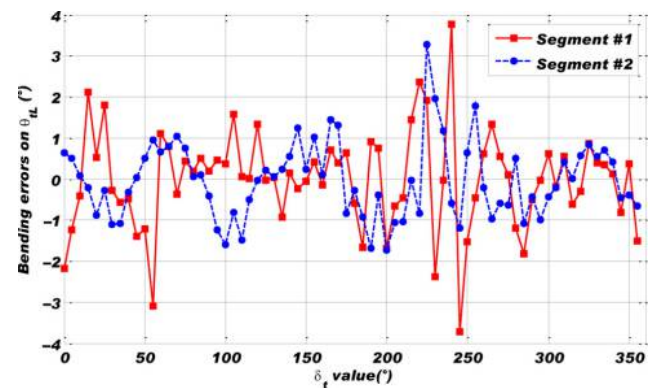
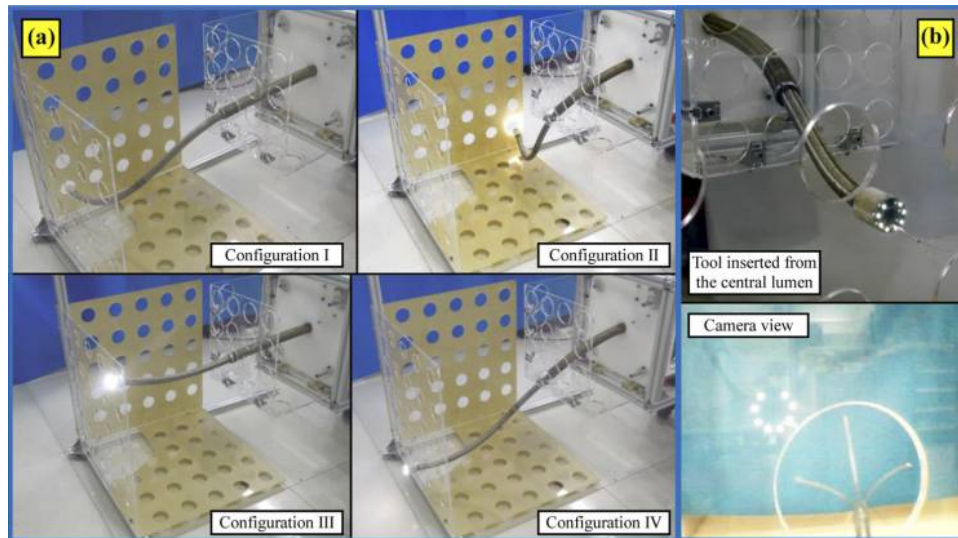


Figure 13 Explore the mockup cavity**Notes:** (a) Different poses of the manipulator, with (b) an endoscopic tool inserted

adjust the manipulator according to the visual guidance. For other intra-cavity applications that require high positioning accuracy, a distal orientation sensing feedback might be needed.

5.2 Motion capabilities and cavity inspection

After motion compensations were implemented, the manipulator was controlled using the 3D joystick as shown in Figure 9 to explore the mockup cavity, as shown in Figure 13. The mockup cavity in Figure 13 is only one-quarter size of the cavity in Figure 3. It is enough to verify the motion capabilities of the manipulator, as the mockup cavity is symmetrical with respect to its center.

The continuum manipulator was first completely housed inside the housing. It was then placed to the entrance of the mockup cavity. Segment 1 was extruded to enter the cavity, under the visual guidance from the vision unit. Even without any other sources of lights, the LEDs provided enough illumination of the field of view of the camera chip.

Through the holes in the Frame A, Segment 2 was extruded to reach various holes in the Frame B. The poses of the manipulator in Figure 13(a) correspond to the simulated poses in Figure 4. The poses look slightly different because of the different viewing angles of the simulation plots in Figure 4 and the pictures in Figure 13(a).

An endoscopic tool could be inserted through the central lumen to pick up an object at the remote location as shown in Figure 13(b). The visual feedback from the camera chip could guide the task. Other exchangeable tools, such as welding guns or laser cutting tips, could also be inserted.

The manipulator could be programmed to reach the holes in the Frame B in a specific sequence automatically, using the control panel to teach the manipulator to repeat the executed trajectories. This could potentially greatly facilitate several route inspection tasks in the aviation industry, such as the inspection of loose or missing rivets and the checking and removal of foreign objects. With the possibility of inserting

other exchangeable tools, more tasks could be possibly automated and performed in a more accurate and convenient manner.

The experiments of cavity exploration might seem simple but the need for such a motion and function is sincere for the checking and removal of small foreign objects. The hope is that engineers in the aviation industry could be inspired by the presented results and they could use this technology in their particular applications.

6. Conclusions and future work

This paper reports the design and construction of a dexterous continuum manipulator for exploration and task execution in confined spaces.

The manipulator's structure was first synthesized based on the kinematics model. Simulations were then performed to confirm its capability of navigating inside the mockup cavity to reach various remote locations. Using the concept of dual continuum mechanisms, the design of the continuum manipulator was materialized. Details of the continuum segments, the actuation unit, the vision unit, the control infrastructure and the user interface are presented.

After motion calibrations and actuation compensations, the motion capabilities of the manipulator were verified via a series of experiments. Under the integrated visual guidance and illumination, the manipulator could reach all the desired locations. Exchangeable endoscope tools can be deployed through the central lumen to perform inspections or manipulation tasks at those remote locations in confined spaces.

This continuum manipulator, as a multi-functional endoscopic platform, could potentially greatly facilitate several route inspection tasks in the aviation industry, such as the guided assembling, the inspection of loose or missing rivets, the checking and removal of foreign objects. With other exchangeable tools inserted, more tasks, which used to be

challenging and troublesome, could be possibly automated and performed in an accurate and convenient manner. It is hoped that engineers in the aviation industry could be inspired by the presented results to use this technology to define other innovative applications.

As the core contribution, the paper demonstrates that the construction of a one-meter continuum manipulator with a length-over-diameter ratio of 30 for industrial applications is possible, following the elaborated design considerations. Its control and actuation could be achieved effectively using a simple kinematics formulation without the implementation of advanced nonlinear mechanics. These results would widen the applicability of the continuum manipulator technology.

Future work mainly includes the implementation of possible improvements of the manipulator's current construction. For example, there is quite some friction inside the manipulator structure. The bending discrepancy caused by the friction could accumulate to an obvious level. Now the manipulator shall be straightened after a few runs to eliminate these accumulated errors. It is desired to further reduce the friction, via better surface finishes and further adjusted manufacturing tolerances. What is more, the user input scheme shall be modified for better intuitiveness. This will allow more efficient teaching of the manipulator for repeated motions and quicker exploration of an unfamiliar cavity.

References

- Anderson, V.C. and Horn, R.C. (1970), "Tensor arm manipulator", United States Patent Application.
- Bai, S. (2014), "Shape modeling of continuous-curvature continuum robots", in Thomas, F. and Gracia, A.P. (Eds), *Computational Kinematics*, Springer, Netherlands, pp. 75-83.
- Buckingham, R., Chitrakaran, V., Conkie, R., Ferguson, G., Graham, A., Lazell, A., Lichon, M., Parry, N., Pollard, F., Kayani, A., Redman, M., Summers, M. and Green, B. (2007), "Snake-arm robots: a new approach to aircraft assembly", SAE Aerotech Congress, Los Angeles, CA.
- Buckingham, R. and Graham, A. (2012), "Nuclear snake-arm robots", *Industrial Robot: An International Journal*, Vol. 39 No. 1, pp. 6-11.
- Camarillo, D.B., Milne, C.F., Carlson, C.R., Zinn, M.R. and Salisbury, J.K. (2008), "Mechanics modeling of tendon-driven continuum manipulators", *IEEE Transactions on Robotics*, Vol. 24 No. 6, pp. 1262-1273.
- Degani, A., Choset, H., Wolf, A. and Zenati, M. (2007), "Highly Articulated Robotic Probe for Minimally Invasive Surgery", *IEEE International Conference on Robotics and Automation (ICRA)*, Orlando, FL, 15-19 May, pp. 4167-4172.
- Dupont, P.E., Lock, J., Itkowitz, B. and Butler, E. (2010), "Design and control of concentric-tube robots", *IEEE Transactions on Robotics*, Vol. 26 No. 2, pp. 209-225.
- Hirose, S. and Ma, S. (1991), "Coupled tendon-driven multijoint manipulator", *IEEE International Conference on Robotics and Automation (ICRA)*, Sacramento, CA, 9-11 April, pp. 1268-1275.
- Jones, B.A. and Walker, I.D. (2006), "Kinematics for multisection continuum robots", *IEEE Transactions on Robotics and Automation*, Vol. 22 No. 1, pp. 43-55.
- Kim, Y.-J., Cheng, S., Kim, S. and Iagnemma, K. (2013), "A novel layer jamming mechanism with tunable stiffness capability for minimally invasive surgery", *IEEE Transactions on Robotics*, Vol. 29 No. 4, pp. 1031-1042.
- Loeve, A.J., Bosma, J.H., Breedveld, P., Dodou, D. and Dankelman, J. (2010), "Polymer rigidity control for endoscopic shaft-guide 'plastolock' – a feasibility study", *Journal of Medical Devices*, Vol. 4 No. 4, pp. 045001-045006.
- Loeve, A.J., Plettenburg, D.H., Breedveld, P. and Dankelman, J. (2012), "Endoscope shaft-rigidity control mechanism: 'FORGUIDE'", *IEEE Transactions on Biomedical Engineering*, Vol. 59 No. 2, pp. 542-551.
- McMahon, W., Chitrakaran, V., Csencsits, M., Dawson, D.M., Walker, I.D., Jones, B.A., Pritts, M., Dienno, D., Grissom, M. and Rahn, C.D. (2006), "Field trials and testing of the octarm continuum manipulator", *IEEE International Conference on Advanced Robotics (ICAR)*, Orlando, FL, 15-19 May, pp. 2336-2341.
- Ma, S., Kobayashi, I., Hirose, S. and Yokoshima, K. (2002), "Control of a multijoint manipulator 'Moray arm'", *IEEE/ASME Transactions on Mechatronics*, Vol. 7 No. 3, pp. 304-317.
- Paljug, E., Ohm, T. and Hayati, S. (1995), "The JPL serpentine robot: a 12 DOF system for inspection", *IEEE International Conference on Robotics and Automation (ICRA)*, Washington, DC, pp. 3143-3148.
- Rolf, M. and Steil, J.J. (2012), "Constant curvature continuum kinematics as fast approximate model for the bionic handling assistant", *IEEE/RSJ International Conference on Intelligent Robots and Systems (IROS)*, Vilamoura, Algarve, 7-12 October, pp. 3440-3446.
- Rone, W.S. and Ben-Tzvi, P. (2014), "Mechanics modeling of multisegment rod-driven continuum robots", *Journal of Mechanisms and Robotics*, Vol. 6 No. 4, p. 41006.
- Rucker, D.C. and Webster, R.J. (2011), "Statics and dynamics of continuum robots with general tendon routing and external loading", *IEEE Transactions on Robotics*, Vol. 27 No. 6, pp. 1033-1044.
- Simaan, N., Xu, K., Kapoor, A., Wei, W., Kazanzides, P., Flint, P. and Taylor, R.H. (2009), "Design and integration of a telerobotic system for minimally invasive surgery of the throat", *International Journal of Robotics Research*, Vol. 28 No. 9, pp. 1134-1153.
- Suzumori, K., Iikura, S. and Tanaka, H. (1991), "Development of flexible microactuator and its applications to robotic mechanisms", *IEEE International Conference on Robotics and Automation (ICRA)*, Sacramento, CA, 9-11 April, pp. 1622-1627.
- Webster, R.J. and Jones, B.A. (2010), "Design and kinematic modeling of constant curvature continuum robots: a review", *International Journal of Robotics Research*, Vol. 29 No. 13, pp. 1661-1683.
- Wolf, A., Brown, H.B., Casciola, R., Costa, A., Schwerin, M., Shamas, E. and Choset, H. (2003), "A mobile hyper redundant mechanism for search and rescue tasks", *IEEE/RSJ International Conference on Intelligent Robots and Systems (IROS)*, Las Vegas, NV, pp. 2889-2895.
- Xu, K., Fu, M. and Zhao, J. (2014), "An experimental kinematic comparison between continuum manipulators with structural variations", *IEEE International Conference on*

- Robotics and Automation (ICRA)*, Hong Kong, 31 May-7 June, pp. 3258-3264.
- Xu, K. and Simaan, N. (2006), "Actuation compensation for flexible surgical snake-like robots with redundant remote actuation", *IEEE International Conference on Robotics and Automation (ICRA)*, Orlando, FL, May, pp. 4148-4154.
- Xu, K. and Simaan, N. (2008), "An investigation of the intrinsic force sensing capabilities of continuum robots", *IEEE Transactions on Robotics*, Vol. 24 No. 3, pp. 576-587.
- Xu, K. and Simaan, N. (2010a), "Analytic formulation for the kinematics, statics and shape restoration of multibackbone continuum robots via elliptic integrals", *Journal of Mechanisms and Robotics*, Vol. 2 No. 1, pp. 1-13.
- Xu, K. and Simaan, N. (2010b), "Intrinsic wrench estimation and its performance index of multi-segment continuum robots", *IEEE Transactions on Robotics*, Vol. 26 No. 3, pp. 555-561.
- Xu, K., Zhao, J. and Fu, M. (2015), "Development of the SJTU unfoldable robotic system (SURS) for single port laparoscopy", *IEEE/ASME Transactions on Mechatronics*, Vol. 20 No. 5, pp. 2133-2145.
- Yagi, A., Matsumiya, K., Masamune, K., Liao, H. and Dohi, T. (2006), "Rigid-flexible outer sheath model using slider linkage

- locking mechanism and air pressure for endoscopic surgery", *International Conference on Medical Image Computing and Computer-Assisted Intervention (MICCAI)*, Copenhagen, 1-6 October, pp. 503-510.
- Yang, J., Jason, P. and Abdel-Malek, K. (2006), "A hyper-redundant continuous robot", *IEEE International Conference on Robotics and Automation (ICRA)*, Orlando, FL, 15-19 May, pp. 1854-1859.
- Zhao, J., Zheng, X., Zheng, M., Shih, A.J. and Xu, K. (2013), "An endoscopic continuum testbed for finalizing system characteristics of a surgical robot for NOTES procedures", *IEEE/ASME International Conference on Advanced Intelligent Mechatronics (AIM)*, Wollongong, 9-12 July, pp. 63-70.
- Zuo, S., Yamanaka, N., Sato, I., Masamune, K., Liao, H., Matsumiya, K. and Dohi, T. (2008), "MRI-compatible rigid and flexible outer sheath device with pneumatic locking mechanism for minimally invasive surgery", *International Workshop on Medical Imaging and Augmented Reality (MIAR)*, Tokyo, pp. 210-219.

Corresponding author

Kai Xu can be contacted at: k.xu@sjtu.edu.cn